Date of publication xxxx 00, 0000, date of current version xxxx 00, 0000.

Digital Object Identifier 10.1109/ACCESS.2017.DOI

Development of active soft robotic manipulators for stable grasping under slippery conditions

CAI LUO[1], (Senior Member, IEEE), KE WANG[1], GUANGYUAN LI[1], SUCHONG YIN[1], LEIJIAN YU[2], AND ERFU YANG[2].

[1]the Department of Mechanical and Electronic Engineering, China University of Petroleum (East China), Qingdao, China
[2]the Department of Design, Manufacture & Engineering Management, University of Strathclyde, Glasgow, UK.

Corresponding author: Cai Luo (e-mail: tsai.lo.95@ gmail.com).

The work was supported in part by the National Natural Science Foundation of China under Grant 61701541, in part by the Shandong Provincial Natural Science Foundation of China under Grant ZR2017QF003 and in part by the Fundamental Research Funds for the Central Universities under Grant 19CX02021A.

ABSTRACT Due to the requirements of industrial automation, soft manipulators are increasingly used in machinery manufacturing, metallurgy and other fields. Typically, a manipulator is only suited to handle objects in ideal dry conditions, which limits the applications of these actuators. To solve the above shortcomings in traditional grippers, this article presents a friction-enhanced soft manipulator that has good flexibility and high interactivity and safety and is also equipped with a bionic nanofiber array film to provide stronger friction under slippery conditions. A polydimethylsiloxane (PDMS) nanofiber array film for increasing the friction of the soft manipulator was fabricated. A suitable manufacturing method for preparing the nanofiber array film was presented. The contact angle of the prepared nanofiber array film was measured. The experimental results showed that the soft robot manipulator performs extremely well under slippery conditions.

INDEX TERMS soft manipulators, stable grasping, slippery condition

I. INTRODUCTION

ROBOTIC manipulators have a wide range of applications in civil productions and can free people from heavy labor duties [1], [2]. Traditional robots are mainly made from rigid materials. These robots are made to grasp and transport objects in repetitive, cumbersome and dangerous working conditions [3]. However, when grasping fragile objects (fruits, vegetables, biological tissues) or in human-robot interactive working environments, the rigid robot cannot meet the requirements of ensuring human and object safety without the support of complicated control systems [4], [5]. These systems can substantially raise the cost of design and maintenance. With the development of 3D printing technology and materials science, some scientists have begun to use soft materials to design and manufacture robots [5], [6]. This provides a completely new solution to the problem of human-machine interaction and the inflexibility of traditional rigid robots. Scientists and engineers were inspired by bionics to design different soft manipulators [7]. By utilizing and exploiting the mechanical intelligence of soft materials, the actuators can be more adaptable to severe working conditions.

A wide range of manipulation methods have been developed recently to design soft robotic actuators. The GEORGE team at Harvard University developed a new multi-cavity soft manipulator with the support of the Defense Advanced Research Projects Agency (DARPA). The manipulator adaptability is strong, but the stability is not high enough when an object is not gripped [1]. Massachusetts Institute of Technology (MIT)'s Marchese and others designed a multi-joint soft robot and studied the movement of the robot in a free space [8]. To broaden the application range of soft robots, Harvard University's GALLOWAY et al. produced two submarine biological sampling soft robots using multi-cavity structures with fiber reinforcements [9]. Mailand et al. of the Federal Institute of Technology in Lausanne (EPFL), Switzerland studied a type of soft manipulator with a micro-colloid inside [10].

In addition to structural improvements, many researchers have broken through the boundaries of tradition and stud-

ied soft robot materials and manufacturing methods [11], [12]. Diller from Carnegie Mellon University uses magnetic polymers to make soft robots [13]. Controlling the magnetic properties of soft robots allows control of the robot's movements in 3D space. Qi et al. produced a soft robot with pre-programming functions using a 4D multi-material printing technology. MIT's Hyunwoo Yuk and others studied the use of hydrogel-made soft robots, which can hide from their surroundings [9]. Hughes et al. from the University of Cambridge, UK, studied conductive thermoplastics based on tactile sensing [14].

In this article, soft elastomer materials and nanofiber materials are used to design 4-finger manipulators. A self-bending, slip-resistant manipulator is presented, and its modeling and manufacturing are demonstrated. The manipulator is composed of four identical fingers based on the proposed method.

The main novelty in this article is the modification of the surface of a pneumatic actuator to achieve grasping performance under wet or slippery conditions. We then design four soft robotic fingers according to the presented modification. The second contribution is that a 3D model is established, and simulations and experiments are conducted to support the analysis. We expect that other researchers will be able use these results with other types of actuators to design slip-resistant grippers.

II. PNEUMATIC MUSCLE MANIPULATORS

Since soft manipulators are made from soft materials, and the material is generally non-linearly deformed, the conventional driving method for rigid materials is no longer suitable [15], [16]. At present, soft robots include direct transfer of the power from the source to the body (pneumatic) or use a directly deformable drive for control (shape memory alloy).

FIGURE 1: The design of the soft manipulator.

A. DESIGN OF THE PNEUMATIC MANIPULATORS

The commonly used driving methods include the following: pneumatic drive, cable drive, shape memory alloy (SMA), and electroactive polymer (EP) drive [17]–[20]. Comparisons of the four driving modes for soft manipulators can be seen in Table 1.

TABLE 1: Comparisons of the four driving modes for soft manipulators [1], [3], [4].

Attribute	Pneumatic	Cable	SMA	EP
Power Output	Middle	High	Small	Small
Power Consumption	High	Low	High	Low
Response Speed	Fast	Fast	Normal	Fast
Weight	Heavy	Normal	Light	Light
Size	Small	Small	Small	Small
Price	Inexpensive	Expensive	Normal	Inexpensive

The soft manipulator studied requires a large output force to facilitate grasping of an object, and the response speed of the soft robot is required to be fast. It also requires better human-manipulator interaction the capture an object and avoid any damage. The pneumatic drive has been chosen to control the entire soft robot based on the consideration of the soft mechanical hand weight, the energy consumption and price [21].

B. MODELLING OF THE PNEUMATIC MANIPULATORS

After selecting the driving method of the soft manipulator to be pneumatic, a multi-balloon soft robot was designed. The structure is shown in Figure 2:

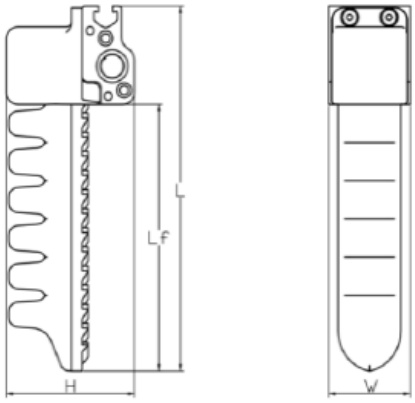

FIGURE 2: Multi-balloon soft robot structure

The multi-balloon soft robot is subject to many influencing factors when it is deformed by force. The deformation of the manipulator is affected by the width, W; length, L; airbag width, a; airbag length, b; airbag height, H; number of airbags, N; and sidewall thickness, dh. The basic parameters in the simulation analysis are as follows: length, 150 mm; width, 16 mm; total height, 12 mm; and number of airbags, 13. The size of each airbag is 10 mm in length, 3 mm in width and 10 mm in height. The distance between each airbag is 10

mm. The back gap has a width of 2 mm and a height of 8 mm. The exploration of the effects of various parameters on the soft robot is based on changing these parameters. During the analysis procedure, the pressure applied inside the soft robot is 0.07 MPa.

The materials that are used to fabricate the manipulators have the properties of a super-elastic [22]. Among the strain energy functions representing super-elastic properties, there are several common models: the Neo-Hooke model [23], the Mooney-Rivlin model [24], and the Ogden model [25]. The most widely used model at this stage is the Neo-Hooke Model. There are two assumptions for materials that can be analysed using the Neo-Hooke model:

- The material is incompressible: even when the material is subjected to a force, it may deform, but the total volume will not change.
- The material is isotropic.

Based on these two assumptions, Rivlin describes the strain energy function as the three main invariants of the Green strain tensor. The expression for I_1, I_2, and I_3 is as follows [26]:

$$W = W(I_1, I_2, I_3) \tag{1}$$

where I_1, I_2, I_3 are three invariants of Green deformation tensor. I_1, I_2, and I_3 can be calculated from:

$$\begin{cases} I_1 = \lambda_1^2 + \lambda_2^2 + \lambda_3^2 \\ I_2 = \lambda_1^2 \cdot \lambda_2^2 + \lambda_1^2 \cdot \lambda_3^2 + \lambda_2^2 \cdot \lambda_3^2 \\ I_3 = \lambda_1^2 \cdot \lambda_2^2 \cdot \lambda_3^2 \\ \lambda_1 = 1 + \varepsilon_i \end{cases} \tag{2}$$

where λ_1 denotes the main elongation ratio and ε_i denotes the main direction strain. Since the material is incompressible, we obtain:

$$I_3 = \lambda_1^2 \cdot \lambda_2^2 \cdot \lambda_3^2 = 1 \tag{3}$$

whereI_1, I_2 can be denoted as:

$$\begin{cases} I_1 = \lambda_1^2 + \lambda_2^2 + \lambda_3^2 \\ I_2 = \frac{1}{\lambda_1^2} + \frac{1}{\lambda_2^2} + \frac{1}{\lambda_3^2} \end{cases} \tag{4}$$

The strain energy expression in the form of the silica Neo-Hooke formula can be rewritten as:

$$W = C_{10}\,(I_1 - 3) \tag{5}$$

1) Effect of balloons with different widths, lengths, and number.

Under the condition that the length of the airbag, b, is constant, there is a relationship between the width of the soft robot and the thickness of the sidewall [27]:

$$W = b + 2d \tag{6}$$

According to Eq. 6, it can be seen that the soft body side wall thickness and the hand width of the soft robot have essentially the same effects on the bending results.

During the simulation, set the width of the soft robot to 14 mm, 16 mm, 18 mm, 20 mm, and 22 mm. The angles of the mechanical arms for different widths are obtained, as shown in Figure 3.

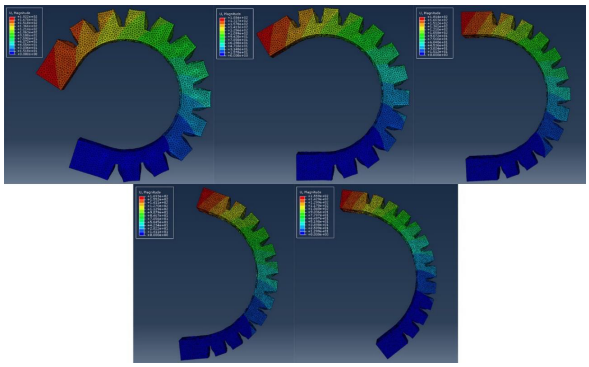

FIGURE 3: Bending angle of soft manipulator with different widths. From top to bottom and left to right, the soft body robot width is 14 mm, 16 mm, 18 mm, 20 mm, and 22 mm.)

Figure 3 shows the bending angle of the soft manipulator for different actuator widths at the same inside pressure of 0.07 MPa. The results are recorded in Table 2.

TABLE 2: Bending angles of a soft manipulator with different actuator widths.

Width W/mm	14	16	18	20	22
Bending angle	258.5°	210.3°	175.8°	155.3°	138.5°

Following the same procedures, the bending angles of the soft manipulator with different parameters such as balloon length, width, depth, number and the spacing between each balloon are summarized in Table 3 through Table 6.

TABLE 3: Bending angles for different balloon lengths.

Length b/mm	6	8	10	12	14
Bending angle	110.1°	165.3°	210.8°	252.5°	289.6°

TABLE 4: Bending angles for different balloon widths.

Width a/mm	2	2.5	3	3.5	4
Bending angle	178.2°	193.4°	210.3°	222.4°	238.4°

It can be seen in Table 4 that as the width of the soft manipulator increases, the bending angle of the actuator gradually changes. As the width of the airbag increases, the bending angle of the soft manipulator is also increased. In Table 5, we see that an increase in the number of airbags has a positive effect on the bending of the soft body manipulator. As shown in Table 6, when the depth of the airbag increases, the bending angle of the soft robot is also increased. It can be seen from Table 7 that as the distance between the airbags increases, the bending angle of the soft manipulator is also increased.

TABLE 5: Bending angles for different numbers of balloons.

Balloon number	11	12	13	14	15
Bending angle	171.4°	190.0°	210.3°	223.6°	240.1°

TABLE 6: Bending angles for different balloon depths.

Depth H/mm	6	7	8	9	10
Bending angle	87.7°	124.8°	161.9°	184.9°	210.3°

2) Manufacture of soft robot actuators

Since the soft robot contains internal airbags, it is impossible to perform casting during the manufacturing process [28]. Thus, the soft robot mold needs to be divided into upper, middle and lower parts.

After the mold is 3D printed, it can be used to manufacture the soft robot. The process is divided into casting, removal and assembly.

The success in casting is directly related to the subsequent steps of molding and assembly. In order to facilitate the processing of the mold before casting, a cotton ball with paraffin oil is used to wipe the inner surface of the mold to ensure that there is a layer of paraffin oil film between the inner surface of the mold and the silica gel. After pouring is completed, due to the existence of a gap between the molds, the mold is sealed with hot melt adhesive to prevent the leakage of the silica gel. This gap can effectively prevent the silica gel from leaking. The mold, after casting, is shown in Figure 4a. After the silica gel is solidified, the silica gel is removed from the mold, as shown in Figure 4b. The cured silica gel forms two parts that are combined to form a complete robotic finger. After the assembly is completed, it is put into an oven for drying. The complete soft robot finger is shown in Figure 4c.

(a) Schematic diagram of the casting process.

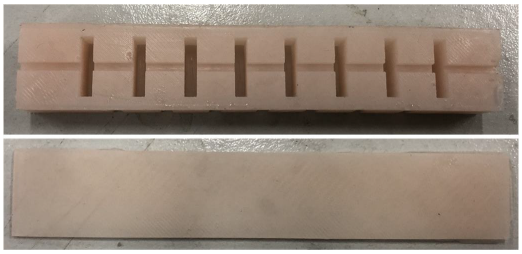

(b) Cured silicone rubber.

(c) Assembled soft manipulator.

FIGURE 4: Process for making a silicone rubber.

III. SLIP RESISTANT GRIPPER TIPS

Animals such as geckos, tree frogs, and bush owls can be found in vertical, wet, and other slippery living environments. Their claws contain microstructures, and the van der Waals forces between these structures and the contact surface keep them from falling [29]. A friction-enhanced material that mimics the preparation of microstructures on the gecko's feet will be presented in the following section.

A. MODELING OF ADHESION OF GECKO FOOT INSPIRED POLYMER MATERIALS.

Since the adhesion mechanism of natural animals is difficult to describe accurately, the approximate small spherical surface is used to indicate its connection to simplify the analysis. The van der Waals adhesion between the end and the plane

TABLE 7: Bending angles for different balloon spacings.

Spacing x/mm	9	10	11	12	13
Bending angle	245.1°	210.3°	175.7°	146.7°	120.6°

can be calculated using the Johnson-Kendall-Roberts (JKR) pull-off formula [30]:

$$F = \frac{3}{2}\pi W_0 R \tag{7}$$

where W_0 denotes the adhesion energy per unit area between two surfaces and R denotes the end radius of curvature. When the fiber is divided into smaller contact areas, the pull-out force will also change according to Eq. 7 and we obtain:

$$F' = n\left(\frac{3}{2}\pi W_0 R'\right) = n\left(\frac{3}{2}\pi W_0 \frac{R}{\sqrt{n}}\right) = \sqrt{n}F \tag{8}$$

where R' denotes end radius of curvature after separation.

Comparing the results of Eq. 7 and Eq. 8, it can be seen that when the contact surface is divided into smaller contact faces, the adhesion to the surface increases. Therefore, by replacing the contact surface between the soft robot and the grasping object with a smaller surface, the gripping ability of the soft robot can be significantly improved. Inspired by the hierarchical structure of a gecko's foot, a fiber structure can be added to the surface of the soft robot to enhance its adhesion [29], [31].

B. FABRICATION AND TESTING OF GECKO BIOMIMETIC NANOFIBER MATERIALS

The nanofiber film has a nano-scale structure on it, which adds a certain difficulty to its preparation. In this paper, a nanofiber film is prepared by template casting, and the preparation process of the method is shown in Figure 5:

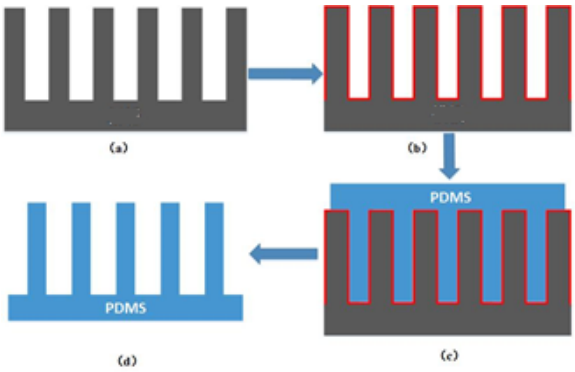

FIGURE 5: Nanofiber array film manufacturing process: (a) Pre-template treatment, (b) template surface treatment, (c) PDMS solution casting, and (d) molding.

After obtaining the PDMS film, it is necessary to verify whether the film has a nanofiber array. According to previous studies [29], [31], PDMS films with nanofiber arrays have certain hydrophobicity, or even superhydrophobicity, and thus, it can be verified whether or not the prepared PDMS film is hydrophobic compared with the untreated PDMS film. The hydrophobic character can be judged by the contact

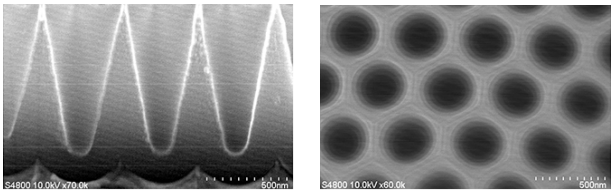

(a) SEM image for the cross section of nanofibre array.

(b) SEM image for the top of nanofibre array.

FIGURE 6: SEM images for nanofibre array film manufacturing.

angle of water droplets on the solid surface. Generally, when the contact angle of the water droplet is greater than 90 degrees, the surface is considered to be hydrophobic. When the angle is larger than 150 degrees, the surface is considered to be superhydrophobic. The hydrophobicity of the nanofiber film was tested according to the hydrophobicity of the surface of the nanofiber. The instrument used was the Theta Lite optical contact angle meter from Biolin Scientific, Sweden. At the time of measurement, 4 liquids were dropped onto the surface of the PDMS film using a syringe attached to the instrument. Then, the contact angle of the water droplet on the surface of the PDMS film was measured by a contact angle measuring instrument. Three points were selected for measurement, and each measurement point was measured five times. The images for different contact points during the measurements are shown in Figure 7.

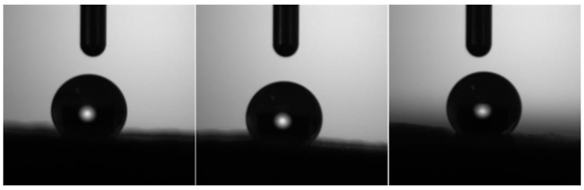

FIGURE 7: Contact angles of water droplets on PDMS nanofiber array film.

The contact angles measured according to the above measurement scheme are recorded in Table 8. In the measurement process, since the solid plane is not necessarily absolutely horizontal, the contact angles on the left and right sides of the droplet are inconsistent. To ensure the accuracy of the measurement results, the left and right sides of the droplet on the solid surface are measured. According to the data in Table 8, the contact angle of water droplets on the surface of the PDMS film is 139.664°, which is close to 150°, and the limit of 150° near the superhydrophobic state indicates that the surface of the PDMS film has good hydrophobicity.

TABLE 8: PDMS nanofiber array film contact angle measurement results.

Test point	Left Angle	Right Angle	Average Angle
Point 1	139.227°	138.812°	139.020°
Point 2	140.382°	140.908°	140.645°
Point 3	138.290°	140.363°	139.327°

In order to enhance the gripping force of the soft robot, a nanofiber array is attached to the fingers of the soft robot, as shown in Figure 8. The area in the red frame in the figure is an additional nanofiber array. The soft robot with the nanofiber array attached was sent to the oven for drying after the array was attached.

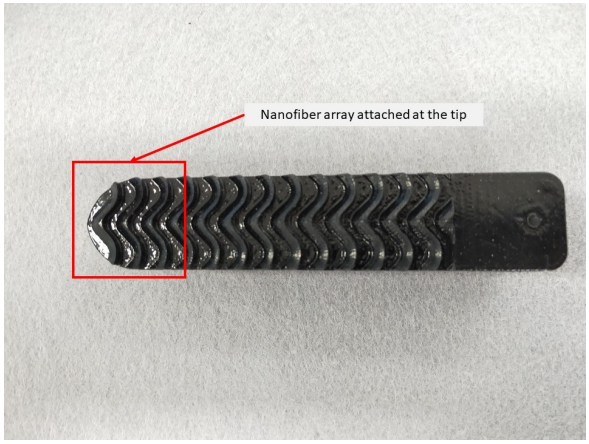

FIGURE 8: Soft manipulator with nanofiber array film attached at the tip.

IV. THE CONTROL SYSTEM OF THE MANIPULATORS

The driving mode of the control system is a pneumatic drive. Under actual working conditions, the gas pressure inside the soft manipulator directly affects the working state of the soft manipulator, which is also the degree of bending. In addition, the gas pressure inside the soft manipulator also affects the gripping force of the soft robot. Therefore, to cope with different work requirements, it is necessary to control the gas pressure inside the soft robot. The control process for the entire control system is obtained according to the requirements of the pneumatic drive control method, as shown in Figure 9.

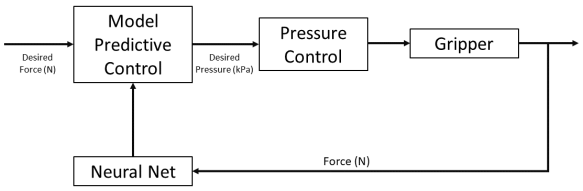

FIGURE 9: Soft manipulator internal gas control process.

A. CONTROLLER DESIGN

The grasping control in slippery condition is a challenge for the proposed manipulators [32]. In this section, a model predictive neural controller (MPNC) has been designed to control the required grasping force.

The cost function can be defined in the following form:

$$\begin{cases} J(k) = \sum_{i=N_1}^{N_2} e^2(k+i) + \rho \sum_{i=1}^{N_u} \Delta u^2(k+i-1) \\ e(k+i) = r(k) - \hat{y}(k+i) \\ \Delta u(k+i-1) = u(k+i-1) - u(k+i-2) \end{cases} \tag{9}$$

where $e(k+i)$ represents the tracking error. $\Delta u(k)$ and $r(k)$ denote the control signal and the reference signal at time K, respectively. $\hat{y}(k+i)$ is the future output prediction. N_1 is the minimum prediction horizon, N_2 represents the prediction horizon, N_u denotes the control horizon, ρ is a factor penalizing.

According to the minimization of a performance criterion, MPC is an iterative optimization strategy repeatedly at each time step t over a finite prediction horizon. The solution to such an optimization control problem depends on current state and leads to an optimal control sequence. The prediction form for the process can be represented as:

$$\begin{aligned} \hat{y}(k+1) =& f(y(k), \ldots, y(k-n_a+1) \\ & u(k-\tau), \ldots, u(k-\tau-n_b+1)) + d(k) \end{aligned} \tag{10}$$

and

$$\begin{cases} d(k) = k_c \varepsilon(k) - d(k-1) \\ \varepsilon(k) = y(k) - \hat{y}(k) \end{cases} \tag{11}$$

where f is a nonlinear function, $y(k)$ is the output at the time k, n_a and n_b denote numbers of past outputs and inputs considered by the model, respectively, τ denotes the time delay, $d(k)$ stands for the disturbance model, k_c is the gain of the disturbance model. k_c is assumed to be equal to 1 and $d(k)$ is assumed to be constant within the prediction horizon.

Neural networks are used to model the nonlinear dynamic process, it can be represented by using feedforward networks with external dynamics as:

$$\begin{cases} f(x) = \sigma_o \left(\boldsymbol{W}_2 \sigma_h \left(\boldsymbol{W}_1 x + \boldsymbol{b}_1 \right) + \boldsymbol{b}_2 \right) \\ x = [y(k), \ldots, y(k-n_a+1) \\ \quad u(k), \ldots, u(k-n_b+1)]^T \end{cases} \tag{12}$$

where $\boldsymbol{W}_1$ and $\boldsymbol{W}_2$ are weight matrices of hidden and output layers, respectively. $\boldsymbol{b}_1$ and $\boldsymbol{b}_2$ are bias vectors of hidden and output units, respectively.

Considering the cost function in Eq.9 and neural network predictor in Eq.12, the MPNC can be defined based on the following constrained finite-horizon optimization:

$$\begin{aligned} J(k) =& \sum_{i=1}^{H_p} [r(k+i) - \hat{y}(k+i)]^T W_i^y [r(k+i) - \hat{y}(k+i)] \\ & + \sum_{j=1}^{H_u} \Delta u(k+j-1)^T W_j^u \Delta u(k+j-1) \end{aligned} \tag{13}$$

subject to

$$\begin{aligned} |\Delta u(k)| &\le \Delta u_{\max} \\ u_{\min} \le u(k) &\le u_{\max} \\ \hat{y}_{\min} \le \hat{y}(k) &\le \hat{y}_{\max} \end{aligned} \tag{14}$$

where r, y, u, and $\hat{y}$ represent the reference, measured output, control input, and predicted output, respectively.

B. STABILITY ANALYSIS

Assuming that $\mathbf{u}(k) = [u(k), u(k+1), \ldots, u(k+H_u-1)]^T$ is the the optimal control at time k found by the optimization approach. Now, let us introduce the suboptimal control $\mathbf{u}_s(k+1)$ postulated at time $k+1$

$$\mathbf{u}_s(k+1) = \underbrace{[u(k+1), \ldots, u(k+H_u-1)}_{H_u-1}, u(k+H_u-1)]^T \tag{15}$$

The control sequence $\mathbf{u}_S(k+1)$ is formed based on the control derived at time k. Therefore, for the suboptimal control $\mathbf{u}_s(t+1)$, the cost function can be defined as

$$\hat{J}_S(t+1) = \rho_1 \sum_{i=2}^{H_p+1} \varepsilon^2(t+i) + \rho_2 \sum_{i=2}^{H_u} \Delta u^2(t+i-1) \tag{16}$$

Then, the difference of cost function $\hat{J}_S(t+1)$ and $\hat{J}(t)$ can be calculated as

$$\hat{J}_S(t+1) - \hat{J}(t) = \rho_1 \left[\varepsilon^2(t+H_p+1) - \varepsilon^2(t+1) \right] - \rho_2 \Delta u^2(t) \tag{17}$$

From Eq.13 and Eq.14, we can get

$$\hat{J}_s(t+1) - \hat{J}(t) = -\rho_1 \varepsilon^2(t+1) - \rho_2 \Delta u^2(t) \le 0 \tag{18}$$

Furthermore, if $\mathbf{u}(t+1)$ is the optimal solution of the optimization problem time $(t+1)$, $J(t+1) \leq \hat{J}_s(t+1)$ as $\mathbf{u_s}(t+1)$ is the suboptimal one. Then, one has

$$\hat{J}(t+1) - \hat{J}(t) \leq \hat{J}_s(t+1) - \hat{J}(t) \leq 0 \qquad (19)$$

Hence, by taking Eq.19, the cost is monotonically decreased with respect to time and control system is stable.

V. EXPERIMENTAL RESULTS AND VALIDATION

Grasping control in slippery conditions is a challenge for the proposed manipulators [32]. In this section, the proposed MPNC approach has been designed using MATLAB to control the required grasping force. The MPNC uses 11-neurons in one hidden layer, 4-delayed plant inputs, 4-delayed plants outputs and was trained for 200 epochs. Data were collected for 1500 seconds at 25 Hz for a series of randoms steps in both pressure and force. From the data, 80% was used for training and 20 % for testing.

To validate the concept of the soft robotic manipulators under slippery condition, we fabricated our pneumatic hand prototype by four fingers. Fig.10 shows the prototype version of the soft gripper are mounted on a NACHI MZ04. In this control system, the feedback force is provided by a force-sensitive resistance (FSR-402) that is mounted on the fingertip of one finger, as shown in Figure 11.

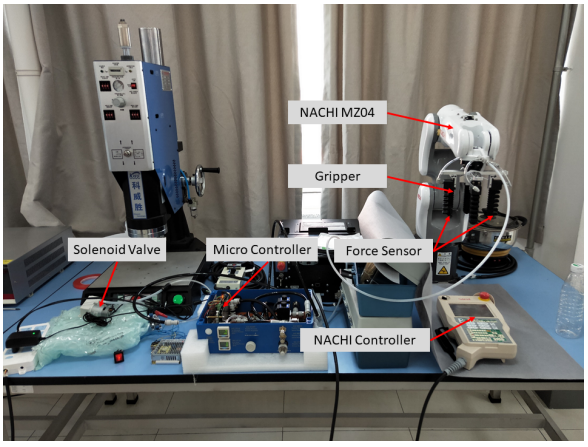

FIGURE 10: The force sensor used for the tests.

FIGURE 11: The force sensor used for the tests.

A group of objects is used with various shapes and weights to examine the effectiveness of the proposed gripper. The objects are used as weights for the gripper and the gripper provides the force (F) to the controller via Arduino Mega 2560; the resulting force is a set point (Fs), the output force is multiplied by 4 to give the sum of the force of the gripper. The control circuit diagram for the soft manipulator is shown in Fig.12. According to Figure 12a, the whole control system is divided into three main parts: the microcontroller that plays the main control role, the pump that provides the gas pressure, and the valve that controls whether the pump and the soft robot are connected internally. The microcontroller is the core unit that can read the pressure value transmitted by the pressure sensor and can control the opening and closing of the pump switch and the valve to control the flow of air to the soft robot.

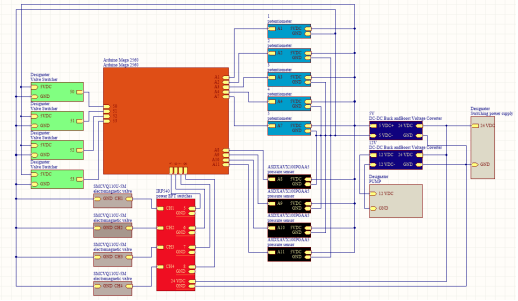

(a) Circuit design for soft manipulator.

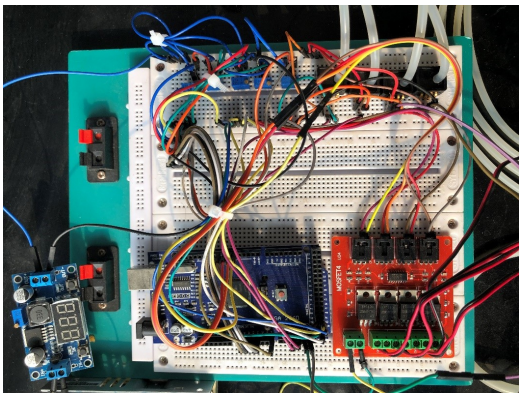

(b) Figure of soft manipulator control circuit.

FIGURE 12: The circuit design and the figure for the soft manipulator.

According to the error sign between the input and the output, the controller will activate either the filling part or the venting part by sending the appropriate duty cycle of the pulse width modulation (PWM) to control the solenoid valve. Fig.13 shows the grasp performance for the object (bottle, cube and glue gun) weights at 20 g, 100 g and 400 g, respectively. The relative maximun pressure for this process is 10 kPa, 30 kPa and 90 kPa, respectively. The relative videos can be seen at:

- Grasp bottle.https://youtu.be/QlmYvkuhY8g
- Grasp cube. https://youtu.be/NWPS2JZ55S8
- Grasp glue gun. https://youtu.be/V1sKlzNAR5w

To further verify the effectiveness of the proposed controller, the comparison experiments were conducted by using PID controller and proposed MPNC controller. The controller is validated by applying step set signals at 2 Hz and

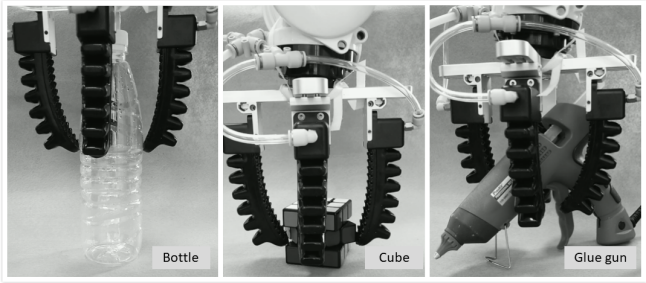

FIGURE 13: Various objects used to examine the effectiveness of the proposed gripper.

1 Hz as shown in Fig.14. It illustrates that the controller is accurate enough to be used for different control frequencies. On the other hand, the time of release is higher than at the time of grasping because the time of grasping because the time needed to vent the muscle is more than the time needed to fill it. This occurs for two reasons: the hysteresis of the soft gripper and the difference between the air pressure inside the actuator and the outside air pressure.

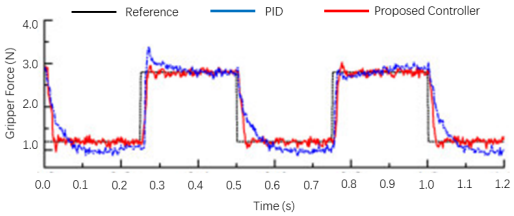

(a) Control frquence at 2 Hz.

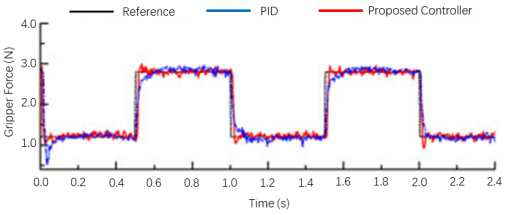

(b) Control frquence at 1 Hz.

FIGURE 14: Force tracking tests for the soft manipulator.

To elucidate the gripping performance of the nanofiber under slippery condition, the comparison experiments were conducted. The maximum lifting weights for various shape of objects (peach, banana and melon) were measured for the proposed nanofiber grippers and grippers without nanofiber.

Fig.15 shows the experimental setup for lifting weight measurements. The objects were put inside a water container in order to maintain their slippery and wet condition. The actuator was manually controlled to grab the objects. Weights were slightly added to the objects if the grab was considered successful and stable. Fig.16 demonstrates the maximum lifting weight differences of the soft manipulators while grasping an object in wet and slippery conditions. The maximum lifting forces of the proposed nanofiber grippers

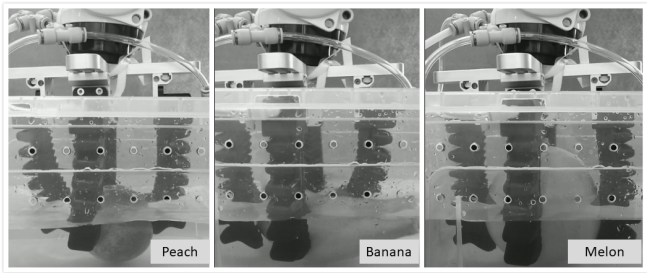

FIGURE 15: Experimental setup for slippery and wet object grasping.

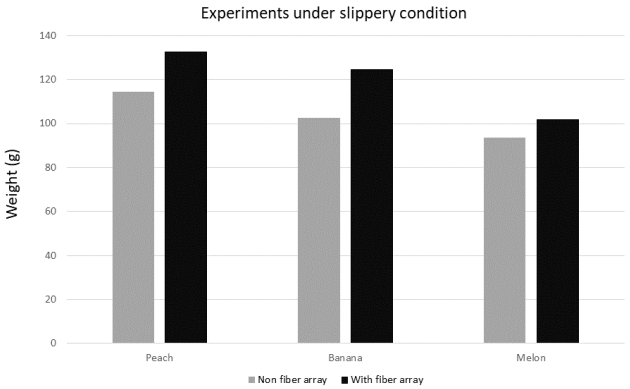

FIGURE 16: The maximum lifting weight grasped by the manipulators under slippery and wet condition.

were higher than the ones without them for all the three objects, which attests an enhanced gripping performance under similar control approach. Due to the wax-coated skin, the maximum grasp weight of melon is lower than the others.

The relative videos can be seen at:

- Grasp peach.https://youtu.be/pDggli3fObg
- Grasp banana. https://youtu.be/Cv3El0e_TEk
- Grasp melon. https://youtu.be/Cv3El0e_TEk

TABLE 9: Comparisons of the nanofiber array for soft manipulators.

Attribute	Gecko fiber	Tree frog fiber	Nano fiber
Underwater	No	No	Yes
Easy to make	Yes	No	Yes
Multi-purpose	No	No	Yes
Size	Small	Small	Small
Price	Inexpensive	Expensive	Normal

VI. CONCLUSIONS AND FUTURE WORK

The grasping and safe handling of objects is a very important issue in robotic applications. The end effector is the part of the robot that has direct contact with the object. Different object dimensions, shapes, materials and weights require different and complex designs of end effectors. The complexity of the design can, in turn, lead to the need for a complex control system. Based on the development of current soft

robots, this paper focuses on how to improve the gripping force of soft robots, prepares materials for improving friction, designs and manufactures soft robots, and develops a control system for soft robots based on an Arduino mega 2560. In this article, a novel soft manipulator with a gecko biomimetic nanofiber array film was presented. In addition, the principle of strong adhesion and friction of the nanofiber array film was analysed. The structure of the friction-enhanced soft-body manipulator is designed. The pneumatic drive is selected as the driving method of the soft manipulator. The control system of the soft manipulator was developed to realize the grasping operation of the object by the soft robot. We have shown experimentally that the designed soft manipulator can robustly obtain the desired grip force under wet and slippery conditions.

ACKNOWLEDGMENT

The authors would like to thank the Oil Industry Training Center in China University of Petroleum for the soft manipulator molding support.

REFERENCES

[1] D. Rus and M. T. Tolley, "Design, fabrication and control of soft robots," Nature, vol. 521, no. 7553, p. 467, 2015.
[2] N. Elango and A. Faudzi, "A review article: investigations on soft materials for soft robot manipulations," The International Journal of Advanced Manufacturing Technology, vol. 80, no. 5-8, pp. 1027–1037, 2015.
[3] J. Hughes, U. Culha, F. Giardina, F. Guenther, A. Rosendo, and F. Iida, "Soft manipulators and grippers: a review," Frontiers in Robotics and AI, vol. 3, p. 69, 2016.
[4] R. Bogue, "Flexible and soft robotic grippers: the key to new markets?" Industrial Robot: An International Journal, vol. 43, no. 3, pp. 258–263, 2016.
[5] R. Pfeifer, M. Lungarella, and F. Iida, "The challenges ahead for bio-inspired'soft'robotics," Communications of the ACM, vol. 55, no. 11, pp. 76–87, 2012.
[6] A. A. Stokes, R. F. Shepherd, S. A. Morin, F. Ilievski, and G. M. Whitesides, "A hybrid combining hard and soft robots," Soft Robotics, vol. 1, no. 1, pp. 70–74, 2014.
[7] G. R. Gossweiler, C. L. Brown, G. B. Hewage, E. Sapiro-Gheiler, W. J. Trautman, G. W. Welshofer, and S. L. Craig, "Mechanochemically active soft robots," ACS applied materials & interfaces, vol. 7, no. 40, pp. 22 431–22 435, 2015.
[8] A. D. Marchese and D. Rus, "Design, kinematics, and control of a soft spatial fluidic elastomer manipulator," The International Journal of Robotics Research, vol. 35, no. 7, pp. 840–869, 2016.
[9] K. C. Galloway, K. P. Becker, B. Phillips, J. Kirby, S. Licht, D. Tchernov, R. J. Wood, and D. F. Gruber, "Soft robotic grippers for biological sampling on deep reefs," Soft robotics, vol. 3, no. 1, pp. 23–33, 2016.
[10] H. Jia, E. Mailand, J. Zhou, Z. Huang, G. Dietler, J. M. Kolinski, X. Wang, and M. S. Sakar, "Universal soft robotic microgripper," Small, vol. 15, no. 4, p. 1803870, 2019.
[11] T. Ranzani, M. Cianchetti, G. Gerboni, I. De Falco, and A. Menciassi, "A soft modular manipulator for minimally invasive surgery: design and characterization of a single module," IEEE Transactions on Robotics, vol. 32, no. 1, pp. 187–200, 2016.
[12] T. G. Thuruthel, E. Falotico, F. Renda, and C. Laschi, "Model-based reinforcement learning for closed-loop dynamic control of soft robotic manipulators," IEEE Transactions on Robotics, vol. 35, no. 1, pp. 124–134, 2019.
[13] E. Diller and M. Sitti, "Three-dimensional programmable assembly by untethered magnetic robotic micro-grippers," Advanced Functional Materials, vol. 24, no. 28, pp. 4397–4404, 2014.
[14] H. Yuk, S. Lin, C. Ma, M. Takaffoli, N. X. Fang, and X. Zhao, "Hydraulic hydrogel actuators and robots optically and sonically camouflaged in water," Nature communications, vol. 8, p. 14230, 2017.
[15] E. Brown, N. Rodenberg, J. Amend, A. Mozeika, E. Steltz, M. R. Zakin, H. Lipson, and H. M. Jaeger, "Universal robotic gripper based on the jamming of granular material," Proceedings of the National Academy of Sciences, vol. 107, no. 44, pp. 18 809–18 814, 2010.
[16] M. Behl, K. Kratz, J. Zotzmann, U. Nöchel, and A. Lendlein, "Reversible bidirectional shape-memory polymers," Advanced materials, vol. 25, no. 32, pp. 4466–4469, 2013.
[17] Y. Yang, Y. Chen, Y. Li, Z. Wang, and Y. Li, "Novel variable-stiffness robotic fingers with built-in position feedback," Soft robotics, vol. 4, no. 4, pp. 338–352, 2017.
[18] H. Rodrigue, B. Bhandari, M.-W. Han, and S.-H. Ahn, "A shape memory alloy–based soft morphing actuator capable of pure twisting motion," Journal of Intelligent Material Systems and Structures, vol. 26, no. 9, pp. 1071–1078, 2015.
[19] H. Dong, E. Asadi, C. Qiu, J. Dai, and I.-M. Chen, "Geometric design optimization of an under-actuated tendon-driven robotic gripper," Robotics and Computer-Integrated Manufacturing, vol. 50, pp. 80–89, 2018.
[20] F. Connolly, P. Polygerinos, C. J. Walsh, and K. Bertoldi, "Mechanical programming of soft actuators by varying fiber angle," Soft Robotics, vol. 2, no. 1, pp. 26–32, 2015.
[21] C. Xiang, J. Guo, Y. Chen, L. Hao, and S. Davis, "Development of a sma-fishing-line-mckibben bending actuator," IEEE Access, vol. 6, pp. 27 183–27 189, 2018.
[22] N. Tan, X. Gu, and H. Ren, "Simultaneous robot-world, sensor-tip, and kinematics calibration of an underactuated robotic hand with soft fingers," IEEE Access, vol. 6, pp. 22 705–22 715, 2018.
[23] L. Treloar, "Stress-strain data for vulcanized rubber under various types of deformation," Rubber Chemistry and Technology, vol. 17, no. 4, pp. 813–825, 1944.
[24] M. Mooney, "A theory of large elastic deformation," Journal of applied physics, vol. 11, no. 9, pp. 582–592, 1940.
[25] R. Ogden, "Elastic deformations of rubberlike solids," in Mechanics of solids. Elsevier, 1982, pp. 499–537.
[26] S. Mahboubi, S. Davis, and S. Nefti-Meziani, "Variable stiffness robotic hand for stable grasp and flexible handling," IEEE Access, vol. 6, pp. 68 195–68 209, 2018.
[27] S. Hartmann and P. Neff, "Polyconvexity of generalized polynomial-type hyperelastic strain energy functions for near-incompressibility," International journal of solids and structures, vol. 40, no. 11, pp. 2767–2791, 2003.
[28] A. Al-Ibadi, S. Nefti-Meziani, and S. Davis, "Active soft end effectors for efficient grasping and safe handling," IEEE Access, vol. 6, pp. 23 591–23 601, 2018.
[29] M. E. Giannaccini, I. Georgilas, I. Horsfield, B. Peiris, A. Lenz, A. G. Pipe, and S. Dogramadzi, "A variable compliance, soft gripper," Autonomous Robots, vol. 36, no. 1-2, pp. 93–107, 2014.
[30] D. Maugis, "Extension of the johnson-kendall-roberts theory of the elastic contact of spheres to large contact radii," Langmuir, vol. 11, no. 2, pp. 679–682, 1995.
[31] M. Manti, T. Hassan, G. Passetti, N. D'Elia, C. Laschi, and M. Cianchetti, "A bioinspired soft robotic gripper for adaptable and effective grasping," Soft Robotics, vol. 2, no. 3, pp. 107–116, 2015.
[32] M. Lazar and O. Pastravanu, "A neural predictive controller for non-linear systems," Mathematics and Computers in Simulation, vol. 60, no. 3-5, pp. 315–324, 2002.